System-by-Design Paradigm-based Synthesis of Spline-Contoured Radomes

M. Salucci, G. Oliveri, M. A. Hannan and A. Massa

Contents

1 [APPROACH 3] Iterative Optimization with PSO + Kriging (no update during optimization) - EXP CORRELATION

1.0.1 Goal

This set of optimizations follows a different approach from the previous one. In this case, we do not update the training set during the optimization. At the end of the optimization, the optimal solutions found by executing different random seeds are ADDED to the original training set. Then, the optimizations are re-executed, by employing the updated training set. This process is then re-iterated until a satisfactory stop criterion is met. More precisely, the iterative approach works as follows

1. **Execute S different optimizations** (S is the number of considered random seeds) using the PSO optimizer **without updating** the training set during the optimization.
2. Compute the **actual fitness** associated to the S optimal solutions;
3. **Add** the S optimal particles and the corresponding actual fitness to the initial training set;
4. Train a new Kriging model, using the incremented training set;
5. Re-execute the S seeds, by only changing the training set used during the optimization for the prediction of the fitness.
6. The iterative process will be stopped when
   (a) A maximum number of iterations I_{max} will be performed;
   (b) The difference between the predicted and actual final fitness for each random seed will go below a certain threshold.

Notes:

- At the end of each loop, the optimized particles are added to the previous training set, without substituting the worst samples already stored inside it. This is done to avoid the removal of training samples that are characterized by an high value of fitness, which are important to correctly model the "bad" regions of the input space during the optimization;
- For comparison purposes, the same initial population and the same random seeds of the previous section have been used. This will allow to have the same fitness evolution up to the iteration where a negative prediction is obtained.
- We don't insert the optimized particles of a given iteration inside the initial swarm of the next iteration, because we want to analyze only the impact of iteratively updating the model.

1.0.2 Parameters

Optimization targets

- Number of variables: $K = 5$;
- Frequency range:
  - Minimum frequency: $f_{min} = 10.75$ $[GHz]$;
  - Maximum frequency: $f_{max} = 14.5$ $[GHz]$;
  - Number of frequency steps: $N_f = 10$ ($\Delta f \simeq 0.42$ $[GHz]$);
  - Central frequency: $f_0 = \frac{f_{min}+f_{max}}{2} \simeq 12.63$ $[GHz]$;
  - Free-space wavelength at the central frequency: $\lambda_0 = \frac{c}{f_0} = 2.38 \times 10^{-2}$ $[m]$;
- Scanning angle range:
  - Minimum scanning angle: $\theta_{min} = 0$ $[deg]$;
  - Maximum scanning angle: $\theta_{max} = 45$ $[deg]$;
  - Number of angular steps: $N_\theta = 4$ ($\theta_1 = 0$ $[deg]$, $\theta_2 = 15$ $[deg]$, $\theta_3 = 30$ $[deg]$, $\theta_4 = 45$ $[deg]$);

PSO **parameters**

- Population dimension: $P = 10$;
- Maximum number of iterations: $I_{max} = 200$;
- Fitness threshold: $\Phi^{th} = 10^{-20}$;
- Inertial weight: $w = 0.4$;
- Constant inertial velocity;
- Exploration coefficient: $c_1 = 2$;
- Exploitation coefficient: $c_2 = 2$;
- Random seed $s = 1, 2, ..., 10$;
- Initialization (generation of the initial swarm): use the same seed for all the optimizations.

Kriging (Gaussian Process Regressor) parameters

- Regression model: constant (Ordinary Kriging);
- Correlation models:
  - Exponential ($p = 1$);

- Initial guess for hyper-parameters θ_h: $\theta_{h,0} = 0.5$, for $h = 1, ..., K$;
- Lower bound for hyper-parameters θ_h: $min\,\{\theta_h\} = 0.1$, for $h = 1, ..., K$;
- Upper bound for hyper-parameters θ_h: $max\,\{\theta_h\} = 20.0$, for $h = 1, ..., K$.

Not-optimized (static) radome parameter

Parameter	**Description**	**Value**
L	Length of the radome	1.59×10^{-1} $[m] \simeq 6.69\ \lambda_0$
D	Base diameter of the radome	1.27×10^{-1} $[m] \simeq 5.35\ \lambda_0$
t_0	Thickness of the base and of the top of the radome	$8.20 \times 10^{-3}[m] \simeq \frac{\lambda_r}{2}$
z_1	z-coordinate of the spline control point 1	$\frac{L-t_0}{6}$
z_2	z-coordinate of the spline control point 2	$2\frac{L-t_0}{6}$
z_3	z-coordinate of the spline control point 3	$3\frac{L-t_0}{6}$
z_4	z-coordinate of the spline control point 4	$4\frac{L-t_0}{6}$
z_5	z-coordinate of the spline control point 5	$5\frac{L-t_0}{6}$
ν	External curvature of the radome ($\nu \in [1, 2]$)	1.449 (tangent ogive)
ε_r	Permittivity of the radome material	2.10 (Teflon)
$\tan\delta_r$	Tangent delta of the radome material	$tan\delta = 3.00 \times 10^{-4}$ @ 10.0 $[GHz]$ (Teflon)
λ_r	Wavelength in the radome material	$\lambda_r \simeq \frac{c}{f_0\sqrt{\varepsilon}} \simeq 1.64 \times 10^{-1}$

Table I: List of non-optimized radome parameters.

Antenna Parameters

- Linear dipole array placed over circular ground plane (PEC)
- Number of array elements: $N_e = 8$
- Dipole length: $l_e = \frac{\lambda_0}{2}$
- Array elements spacing: $d_e = \lambda/2$
- Spacing between the array and the ground plane: $h_e = \frac{\lambda_0}{4}$

Parameters boundaries

Parameter	**Description**	Min	Max
t_1	Radome thickness at the quota $z = z_1$	3.28×10^{-3}[m] $(0.2\lambda_r)$	13.12×10^{-3}[m] $(0.8\lambda_r)$
t_2	Radome thickness at the quota $z = z_2$	3.28×10^{-3}[m] $(0.2\lambda_r)$	13.12×10^{-3}[m] $(0.8\lambda_r)$
t_3	Radome thickness at the quota $z = z_3$	3.28×10^{-3}[m] $(0.2\lambda_r)$	13.12×10^{-3}[m] $(0.8\lambda_r)$
t_4	Radome thickness at the quota $z = z_4$	3.28×10^{-3}[m] $(0.2\lambda_r)$	13.12×10^{-3}[m] $(0.8\lambda_r)$
t_5	Radome thickness at the quota $z = z_5$	3.28×10^{-3}[m] $(0.2\lambda_r)$	13.12×10^{-3}[m] $(0.8\lambda_r)$

Table II: List of all considered boundaries for the optimized radome descriptors.

1.0.3 Predicted fitness vs. iteration index ($s \in [1, 10]$)

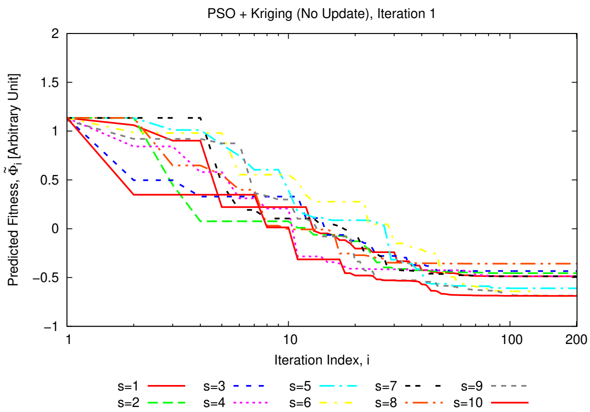

(a) Iteration 1 ($N = 250$)

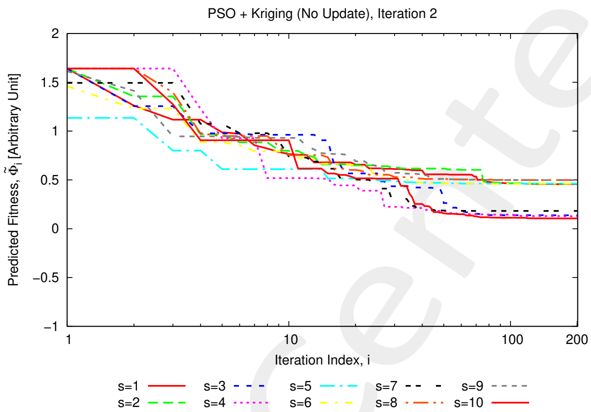

(b) Iteration 2 ($N = 260$)

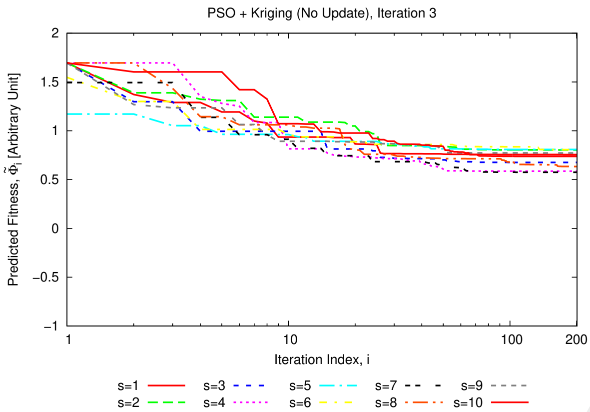

(c) Iteration 3 ($N = 270$)

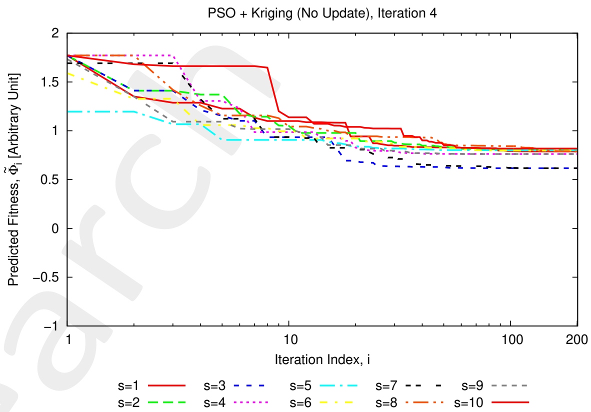

(d) Iteration 4 ($N = 280$)

Figure 1: **Iterations 1-4:** Predicted fitness vs. iteration index, for different random seeds ($s \in [1, 10]$).

1.0.4 Predicted fitness vs. real fitness

Legend

- $\widetilde{\Phi}_0$: Predicted fitness for the best particle of the initial swarm;
- Φ_0: Actual fitness for the best particle of the initial swarm;
- $\widetilde{\Phi}^{opt}$: Predicted fitness for the optimal solution found at the end of the PSO;
- Φ^{opt}: Actual fitness computed for the optimal solution found at the end of the PSO;
- Φ^{opt}_{train}: Best fitness inside the training set at current iteration.

Iteration 1 ($N = 250$ training samples, $\Phi^{opt}_{train} = 1.13$)

	Predicted		**Actual**		
Seed (s)	$\widetilde{\Phi}_0$	$\widetilde{\Phi}^{opt}$	Φ_0	Φ^{opt}	$100\frac{\Phi^{opt}_{train}-\Phi^{opt}}{\Phi^{opt}_{train}}$
1	1.13	-4.88×10^{-1}	2.11	1.62	−43.36
2	1.13	-4.55×10^{-1}	2.11	1.45	−28.32
3	1.13	-4.33×10^{-1}	2.11	1.19	−5.31
4	1.13	-4.88×10^{-1}	2.11	1.62	−43.36
5	1.13	-6.11×10^{-1}	2.11	1.53	−35.40
6	1.13	-6.88×10^{-1}	2.11	1.32	−16.81
7	1.13	-4.88×10^{-1}	2.11	1.62	−43.36
8	**1.13**	$\mathbf{-3.58 \times 10^{-1}}$	**2.11**	**1.07**	**5.31**
9	1.13	-6.86×10^{-1}	2.11	1.33	−17.70
10	1.13	-6.88×10^{-1}	2.11	1.32	−16.81

Table III: **Iteration 1:** Number of updates during the optimization, initial and final predicted fitness and associated real fitness, for each considered random seed $s \in [1, 10]$.

Iteration 2 ($N = 260$ training samples, $\Phi^{opt}_{train} = 1.07$ (from iteration 1))

Note that $\widetilde{\Phi}_0$ is different from iteration 1, because the training set has been updated.

	Predicted		**Actual**		
Seed (s)	$\widetilde{\Phi}_0$	$\widetilde{\Phi}^{opt}$	Φ_0	Φ^{opt}	$100\frac{\Phi^{opt}_{train}-\Phi^{opt}}{\Phi^{opt}_{train}}$
1	1.64	4.56×10^{-1}		8.65×10^{-1}	19.16
2	1.64	4.60×10^{-1}		8.51×10^{-1}	20.47
3	1.64	1.37×10^{-1}		1.18	−10.28
4	1.64	1.28×10^{-1}		1.28	−19.63
5	1.64	4.62×10^{-1}		8.53×10^{-1}	20.28
6	1.64	4.60×10^{-1}		8.51×10^{-1}	20.47
7	1.64	1.82×10^{-1}		1.23	−14.95
8	1.64	4.98×10^{-1}		8.71×10^{-1}	18.60
9	**1.64**	$\mathbf{4.98 \times 10^{-1}}$		$\mathbf{8.16 \times 10^{-1}}$	**23.74**
10	1.64	1.05×10^{-1}		1.07	0.00

Table IV: **Iteration 2:** Number of updates during the optimization, initial and final predicted fitness and associated real fitness, for each considered random seed $s \in [1, 10]$.

Iteration 3 ($N = 270$ **training samples,** $\Phi_{train}^{opt} = 8.16 \times 10^{-1}$ **(from iteration 2))**

	Predicted		**Actual**		
Seed (s)	$\widetilde{\Phi}_0$	$\widetilde{\Phi}^{opt}$	Φ_0	Φ^{opt}	$100\frac{\Phi_{train}^{opt}-\Phi^{opt}}{\Phi_{train}^{opt}}$
1	1.70	7.56×10^{-1}		1.05	-28.68
2	1.70	8.03×10^{-1}		8.35×10^{-1}	-2.33
3	1.70	6.76×10^{-1}		1.25	-53.19
4	1.70	5.87×10^{-1}		1.27	-55.64
5	1.70	8.08×10^{-1}		8.56×10^{-1}	-4.90
6	1.70	8.06×10^{-1}		8.45×10^{-1}	-3.55
7	1.70	5.75×10^{-1}		1.25	-53.19
8	1.70	6.34×10^{-1}		9.98×10^{-1}	-22.30
9	**1.70**	$\mathbf{7.72 \times 10^{-1}}$		$\mathbf{8.33 \times 10^{-1}}$	$\mathbf{-2.08}$
10	1.70	7.38×10^{-1}		1.01	-23.77

Table V: **Iteration 3:** Number of updates during the optimization, initial and final predicted fitness and associated real fitness, for each considered random seed $s \in [1, 10]$.

Iteration 4 ($N = 270$ **training samples,** $\Phi_{train}^{opt} = 8.16 \times 10^{-1}$ **(from iteration 2))**

	Predicted		**Actual**		
Seed (s)	$\widetilde{\Phi}_0$	$\widetilde{\Phi}^{opt}$	Φ_0	Φ^{opt}	$100\frac{\Phi_{train}^{opt}-\Phi^{opt}}{\Phi_{train}^{opt}}$
1	1.77	7.89×10^{-1}		9.87×10^{-1}	-20.96
2	1.77	8.08×10^{-1}		1.00	-22.55
3	1.77	6.16×10^{-1}		1.22	-49.51
4	1.77	7.62×10^{-1}		8.43×10^{-1}	-3.31
5	1.77	8.00×10^{-1}		8.76×10^{-1}	-7.35
6	1.77	7.97×10^{-1}		9.38×10^{-1}	-14.95
7	1.77	6.17×10^{-1}		1.22	-49.51
8	1.77	7.87×10^{-1}		9.18×10^{-1}	-12.50
9	**1.77**	$\mathbf{7.62 \times 10^{-1}}$		$\mathbf{8.43 \times 10^{-1}}$	$\mathbf{-3.31}$
10	1.77	8.18×10^{-1}		9.20×10^{-1}	-12.74

Table VI: **Iteration 4:** Number of updates during the optimization, initial and final predicted fitness and associated real fitness, for each considered random seed $s \in [1, 10]$.

Statistics (over $S = 10$ **seeds)**

	Predicted				**Actual**			
Iteration	$min\left\{\widetilde{\Phi}^{opt}\right\}$	$max\left\{\widetilde{\Phi}^{opt}\right\}$	$avg\left\{\widetilde{\Phi}^{opt}\right\}$	$std\left\{\widetilde{\Phi}^{opt}\right\}$	$min\left\{\Phi^{opt}\right\}$	$max\left\{\Phi^{opt}\right\}$	$avg\left\{\Phi^{opt}\right\}$	$std\left\{\Phi^{opt}\right\}$
1	-6.88×10^{-1}	-3.58×10^{-1}	-5.38×10^{-1}	1.14×10^{-1}	1.07	1.62	1.41	1.84×10^{-1}
2	1.05×10^{-1}	4.98×10^{-1}	3.39×10^{-1}	1.65×10^{-1}	8.16×10^{-1}	1.28	9.87×10^{-1}	1.75×10^{-1}
3	5.75×10^{-1}	8.08×10^{-1}	7.16×10^{-1}	8.63×10^{-2}	8.33×10^{-1}	1.27	1.02	1.72×10^{-1}
4	6.16×10^{-1}	8.18×10^{-1}	7.55×10^{-1}	7.15×10^{-2}	8.43×10^{-1}	1.22	9.77×10^{-1}	1.32×10^{-1}

Table VII: **Iterations 1-4:** Statistics (min, max, average and standard deviation) of the predicted and actual fitness obtained over $S = 10$ seeds.

Difference between predicted and actual fitness

- Mean Absolute Error (MAE): $MAE = \frac{1}{S}\sum_{s=1}^{S}\left|\widetilde{\Phi}_s^{opt} - \Phi_s^{opt}\right|$
- Normalized Mean Error (NME): $NME = \frac{1}{S}\sum_{s=1}^{S}\frac{\left|\widetilde{\Phi}_s^{opt} - \Phi_s^{opt}\right|}{\left|\Phi_s^{opt}\right|}$
- Matching Error (ME): $ME = \frac{1}{S}\frac{\sum_{s=1}^{S}\left|\widetilde{\Phi}_s^{opt} - \Phi_s^{opt}\right|^2}{\sum_{s=1}^{S}\left|\Phi_s^{opt}\right|^2}$

Iteration	MAE	NME	ME
1	1.94	1.39	1.90
2	6.48×10^{-1}	6.21×10^{-1}	5.29×10^{-1}
3	3.05×10^{-1}	2.67×10^{-1}	1.45×10^{-1}
4	2.22×10^{-1}	2.07×10^{-1}	9.02×10^{-2}

Table VIII: **Iterations 1-4:** Difference between final predicted and actual fitness for all the considered random seeds.

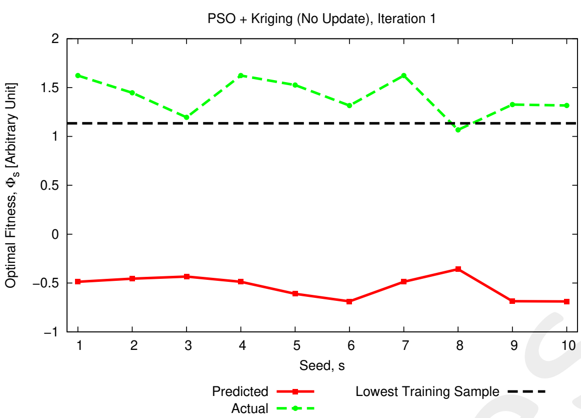

(a) Iteration 1

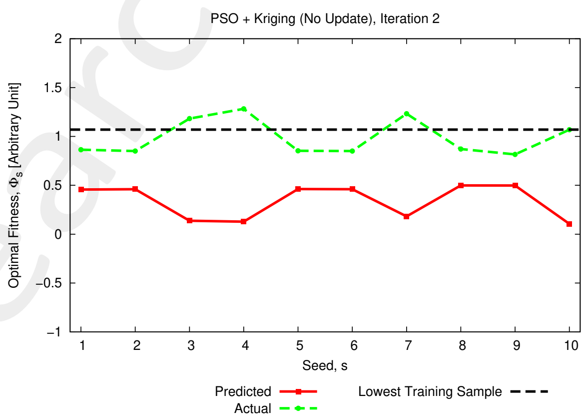

(b) Iteration 2

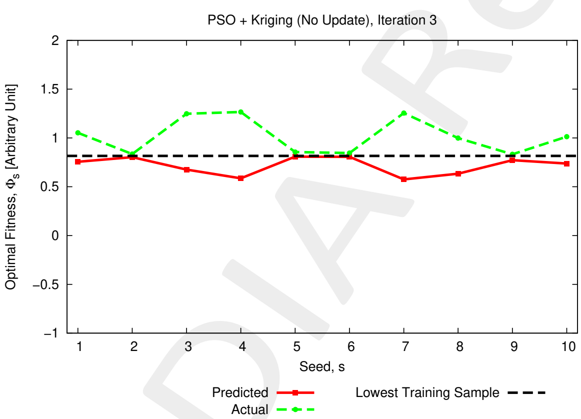

(c) Iteration 3

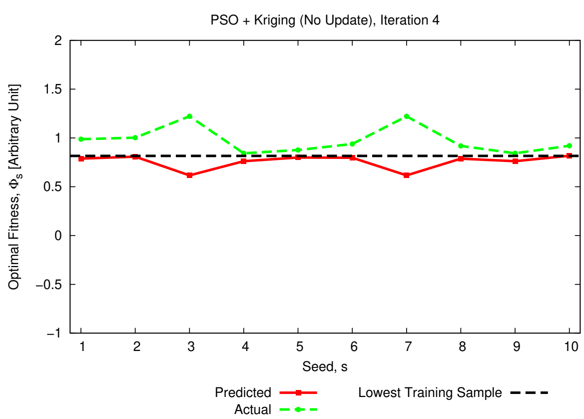

(d) Iteration 4

Figure 2: **Iterations 1-4:** Predicted and actual final fitness for different random seeds ($s \in [1, 10]$).

1.0.5 Optimized parameters $(t_1^{opt}, ..., t_5^{opt})$ vs. seed

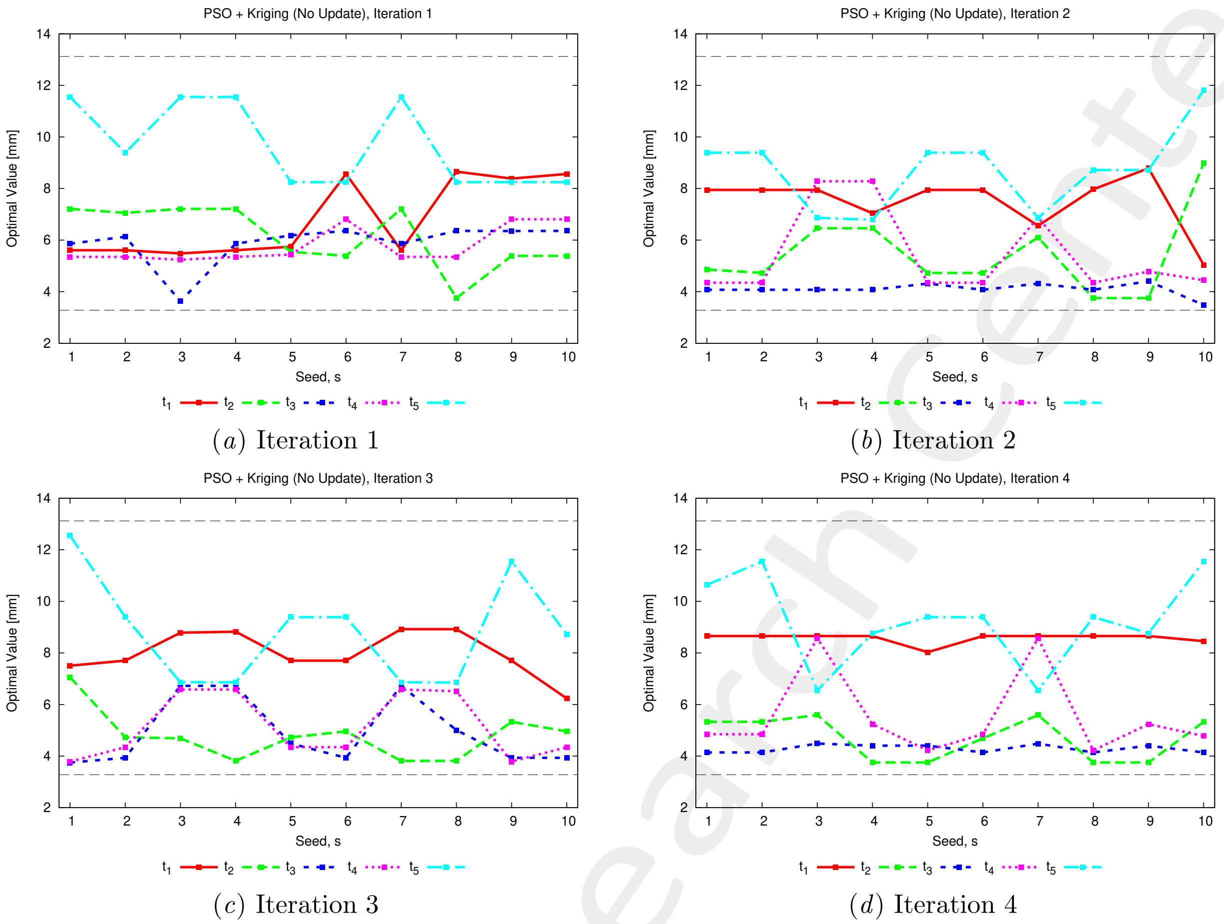

(a) Iteration 1 (b) Iteration 2 (c) Iteration 3 (d) Iteration 4

Figure 3: **Iterations 1-4:** Predicted and actual final fitness for different random seeds ($s \in [1, 10]$).

1.0.6 Best solution found (min. actual fitness)

1. **Iteration 1**

    - Seed: $s = 8$;
    - True fitness: $\Phi^{opt} = 1.07$;
    - Average BSE error: $BSE_{avg} = \sqrt{\Phi^{opt}} = 1.03$ [deg].

2. **Iteration 2**

    - Seed: $s = 9$;
    - True fitness: $\Phi^{opt} = 8.16 \times 10^{-1}$ (**BEST SOLUTION SO FAR**);
    - Average BSE error: $BSE_{avg} = \sqrt{\Phi^{opt}} = 0.90$ [deg].

3. **Iteration 3**

    - Seed: $s = 9$;
    - True fitness: $\Phi^{opt} = 8.33 \times 10^{-1}$;
    - Average BSE error: $BSE_{avg} = \sqrt{\Phi^{opt}} = 0.91$ [deg].

4. **Iteration 4**

    - Seed: $s = 4$ and $s = 9$;
    - True fitness: $\Phi^{opt} = 8.43 \times 10^{-1}$;
    - Average BSE error: $BSE_{avg} = \sqrt{\Phi^{opt}} = 0.92$ [deg].

1.0.7 Analysis of the best solution (Iteration 2, seed $s = 9$, $\Phi^{opt} = 8.16 \times 10^{-1}$)

Optimized parameters ($t_1^{opt}, ..., t_5^{opt}$)

Parameter	Description	Optimized Value [m]	Min [m]	Max [m]
t_1	Radome thickness at the quota $z = z_1$	8.79×10^{-3}	3.28×10^{-3}	13.12×10^{-3}
t_2	Radome thickness at the quota $z = z_2$	3.75×10^{-3}	3.28×10^{-3}	13.12×10^{-3}
t_3	Radome thickness at the quota $z = z_3$	4.41×10^{-3}	3.28×10^{-3}	13.12×10^{-3}
t_4	Radome thickness at the quota $z = z_4$	4.78×10^{-3}	3.28×10^{-3}	13.12×10^{-3}
t_5	Radome thickness at the quota $z = z_5$	8.72×10^{-3}	3.28×10^{-3}	13.12×10^{-3}

Table IX: Optimized parameters for the best seed ($s = 8$).

Pointing error (BSE) vs. frequency

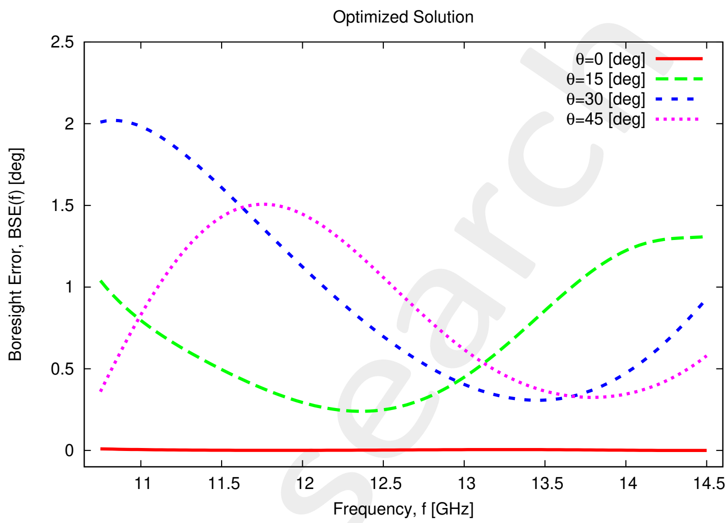

Figure 4: Pointing error (BSE) vs. frequency.

Directivity patterns

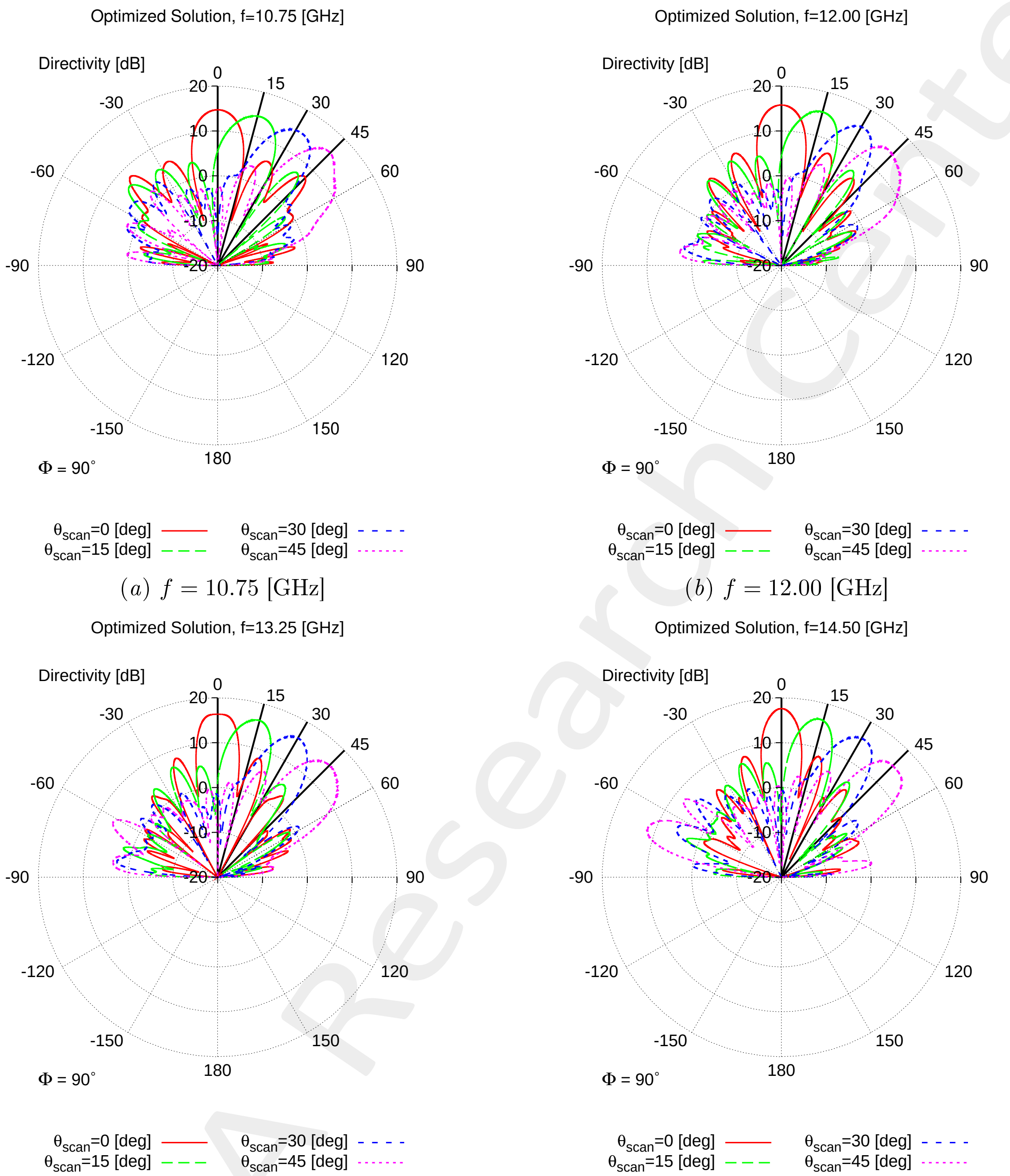

(a) $f = 10.75$ [GHz] (b) $f = 12.00$ [GHz]

(c) $f = 13.25$ [GHz] (d) $f = 14.50$ [GHz]

Figure 5: Radiated pattern for the optimized solution at (a) 10.75 [GHz], (b) 12.00 [GHz], (c) 13.25 [GHz] and (d) 14.50 [GHz].

2 Refining the training set with a MSE-based sampling strategy

2.0.1 Prediction performance with the refined training set

Parameters

Optimization targets

- Number of variables: $K = 5$;
- Frequency range:
  - Minimum frequency: $f_{min} = 10.75$ $[GHz]$;
  - Maximum frequency: $f_{max} = 14.5$ $[GHz]$;
  - Number of frequency steps: $N_f = 10$ ($\Delta f \simeq 0.42$ $[GHz]$);
  - Central frequency: $f_0 = \frac{f_{min}+f_{max}}{2} \simeq 12.63$ $[GHz]$;
  - Free-space wavelength at the central frequency: $\lambda_0 = \frac{c}{f_0} = 2.38 \times 10^{-2}$ $[m]$;
- Scanning angle range:
  - Minimum scanning angle: $\theta_{min} = 0$ $[deg]$;
  - Maximum scanning angle: $\theta_{max} = 45$ $[deg]$;
  - Number of angular steps: $N_\theta = 4$ ($\theta_1 = 0$ $[deg]$, $\theta_2 = 15$ $[deg]$, $\theta_3 = 30$ $[deg]$, $\theta_4 = 45$ $[deg]$);

Kriging (Gaussian Process Regressor) parameters

- Regression model: constant (Ordinary Kriging);
- Correlation model: Exponential ($p = 1$);
- Initial guess for hyper-parameters θ_h: $\theta_{h,0} = 0.5$, for $h = 1, ..., K$;
- Lower bound for hyper-parameters θ_h: $min\{\theta_h\} = 0.1$, for $h = 1, ..., K$;
- Upper bound for hyper-parameters θ_h: $max\{\theta_h\} = 20.0$, for $h = 1, ..., K$;

Incremental training parameters

- Number of available simulations: $S = 250$ (LHS sampling);
- Dimension of the training sets: $N_1 = 20$, $N_{max} = N_L = 200$, step $\Delta N = 20$;

MSE parameters

- Initial training set size: 250 (generated with a LHS);
- Final training set size: 450;

- Number of samples added to the training set for each MSE iteration: 1;
- Number of candidates generated at each MSE iteration: 1000;
- Correlation model: Exponential ($p = 1$);

Not-optimized (static) radome parameter

Parameter	**Description**	**Value**
L	Length of the radome	1.59×10^{-1} $[m] \simeq 6.68$ λ_0
D	Base diameter of the radome	1.27×10^{-1} $[m] \simeq 5.34$ λ_0
t_0	Thickness of the base and of the top of the radome	8.20×10^{-3} $[m]$
z_1	z-coordinate of the spline control point 1	$\frac{L-t_0}{6}$
z_2	z-coordinate of the spline control point 2	$2\frac{L-t_0}{6}$
z_3	z-coordinate of the spline control point 3	$3\frac{L-t_0}{6}$
z_4	z-coordinate of the spline control point 4	$4\frac{L-t_0}{6}$
z_5	z-coordinate of the spline control point 5	$5\frac{L-t_0}{6}$
ν	External curvature of the radome ($\nu \in [1, 2]$)	1.449 (tangent ogive)
ε_r	Permittivity of the radome material	2.10 (Teflon)
$\tan\delta_r$	Tangent delta of the radome material	$tan\delta = 3.00 \times 10^{-4}$ @ 10.0 $[GHz]$ (Teflon)
λ_r	Wavelength in the radome material	$\lambda_r \simeq \frac{c}{f_0\sqrt{\varepsilon}} \simeq 1.64 \times 10^{-1}$

Table X: List of non-optimized radome parameters.

Antenna Parameters

- Linear dipole array placed over circular ground plane (PEC).
- Number of array elements: $N_e = 8$
- Dipole length: $l_e = \frac{\lambda_0}{2}$
- Array elements spacing: $d_e = \lambda/2$
- Spacing between the array and the ground plane: $h_e = \frac{\lambda_0}{4}$

Parameters boundaries

Parameter	**Description**	Min	Max
t_1	Radome thickness at the quota $z = z_1$	3.28×10^{-3} $(0.2 \times \lambda_r)$	13.12×10^{-3} $(0.8 \times \lambda_r)$
t_2	Radome thickness at the quota $z = z_2$	3.28×10^{-3} $(0.2 \times \lambda_r)$	13.12×10^{-3} $(0.8 \times \lambda_r)$
t_3	Radome thickness at the quota $z = z_3$	3.28×10^{-3} $(0.2 \times \lambda_r)$	13.12×10^{-3} $(0.8 \times \lambda_r)$
t_4	Radome thickness at the quota $z = z_4$	3.28×10^{-3} $(0.2 \times \lambda_r)$	13.12×10^{-3} $(0.8 \times \lambda_r)$
t_5	Radome thickness at the quota $z = z_5$	3.28×10^{-3} $(0.2 \times \lambda_r)$	13.12×10^{-3} $(0.8 \times \lambda_r)$

Table XI: List of all considered boundaries for the optimized radome descriptors.

2.0.2 Resulting Training Set

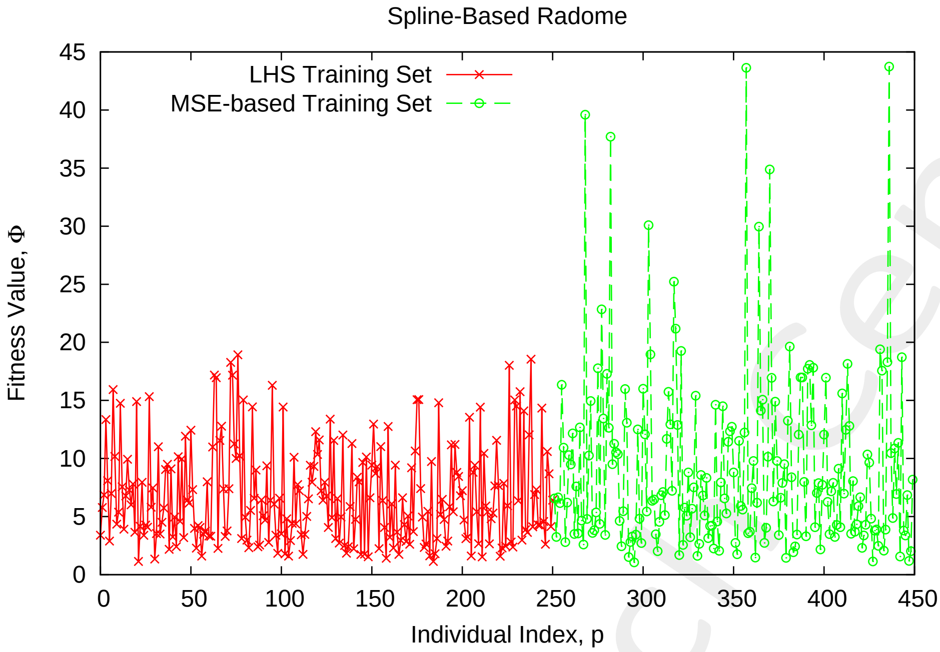

Figure 6: Plot of the starting LHS training samples and the samples belonging to the MSE-based refinement training set.

2.0.3 Predicted Fitness Values

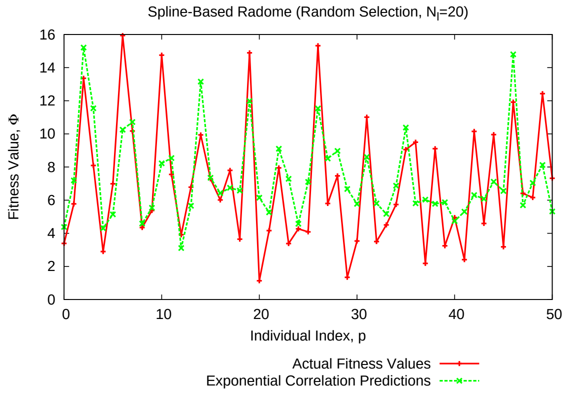

(a) $N = 20$

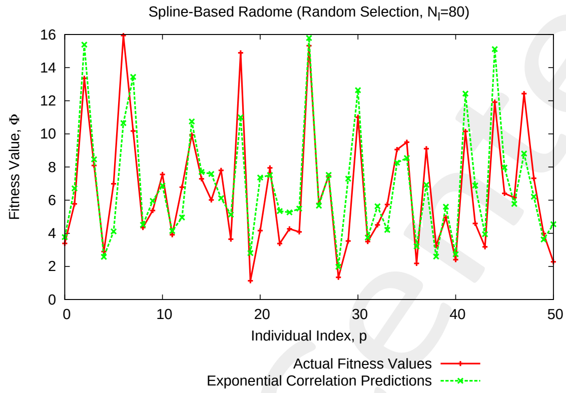

(b) $N = 80$

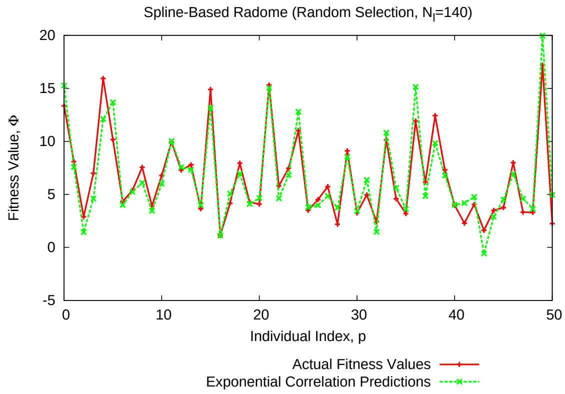

(c) $N = 140$

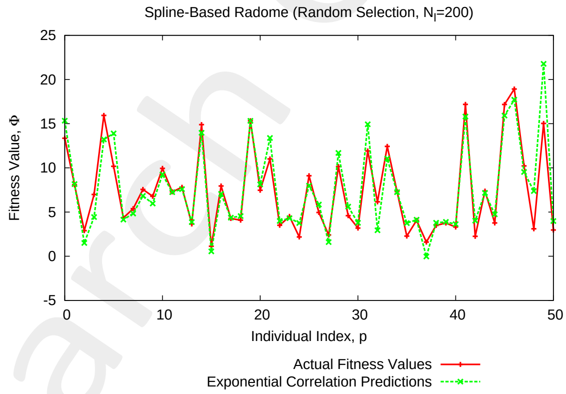

(d) $N = 200$

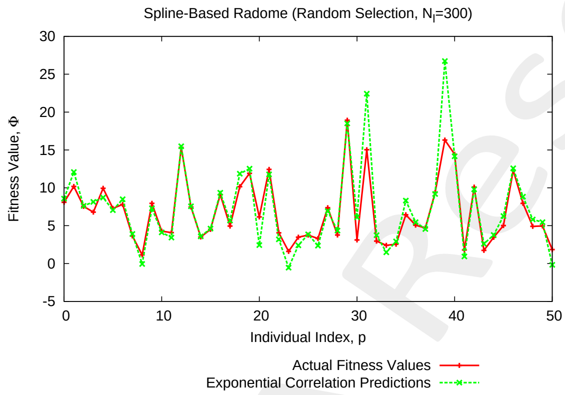

(e) $N = 300$

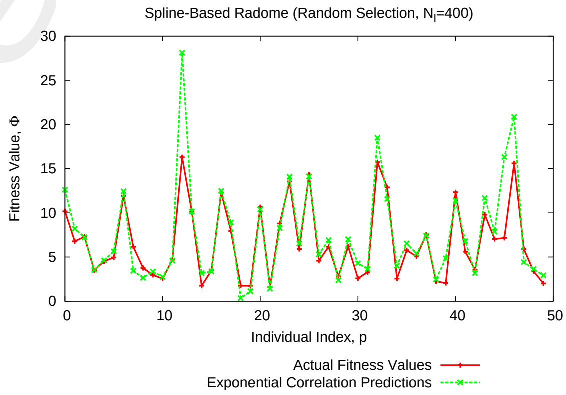

(f) $N = 400$

Figure 7: Actual and predicted functional values of 50 random individuals for different training sizes (N): (a) $N = 20$, (b) $N = 80$, (c) $N = 140$, (d) $N = 200$, (e) $N = 300$ and (f) $N = 400$.

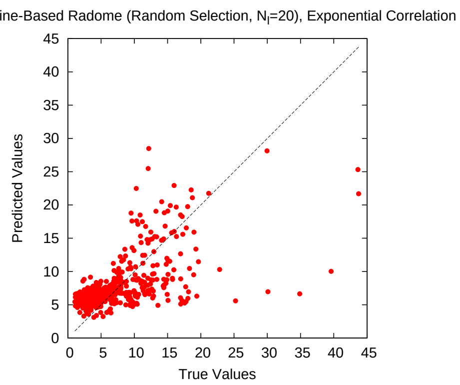

(a) $N = 20$

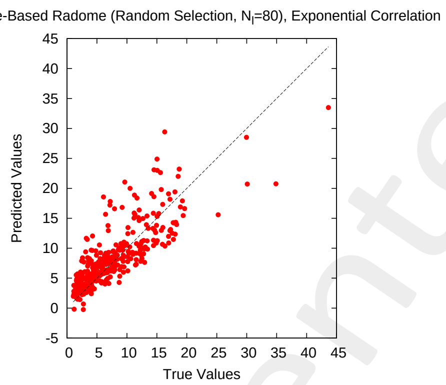

(b) $N = 80$

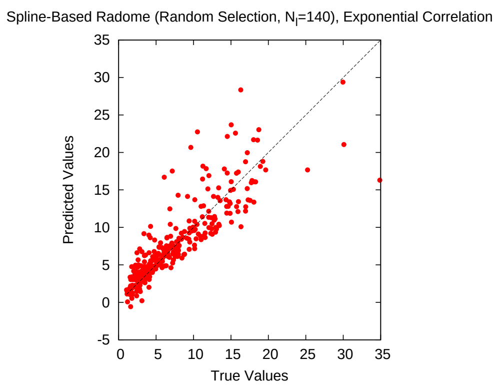

(c) $N = 140$

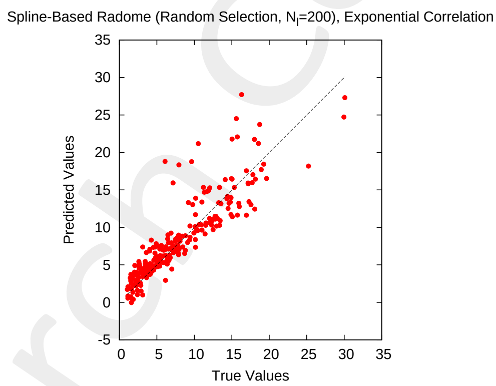

(d) $N = 200$

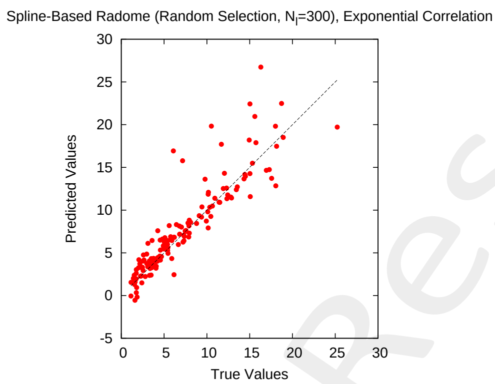

(e) $N = 300$

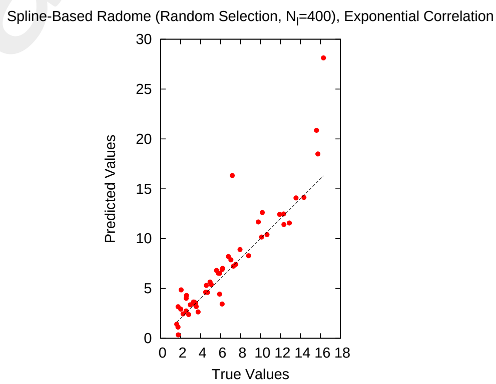

(f) $N = 400$

Figure 8: Plot of predicted vs actual values for different training sizes (N): (a) $N = 20$, (b) $N = 80$, (c) $N = 140$, (d) $N = 200$, (e) $N = 300$ and (f) $N = 400$.

2.0.4 Prediction Error vs Training Size

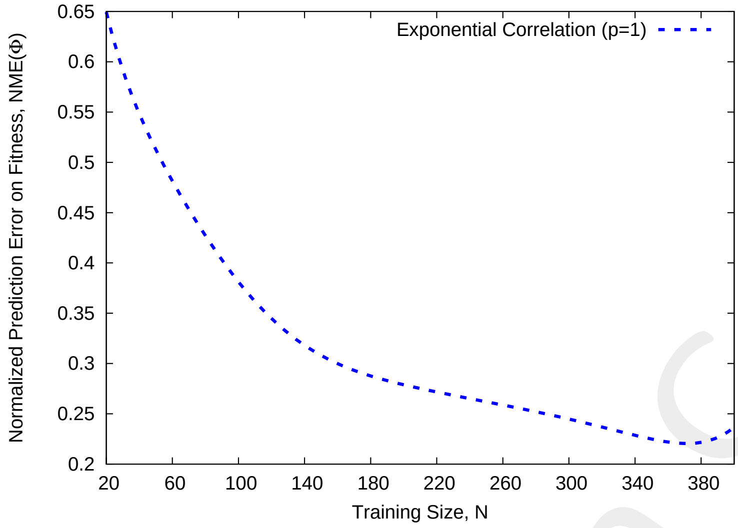

(a) NME

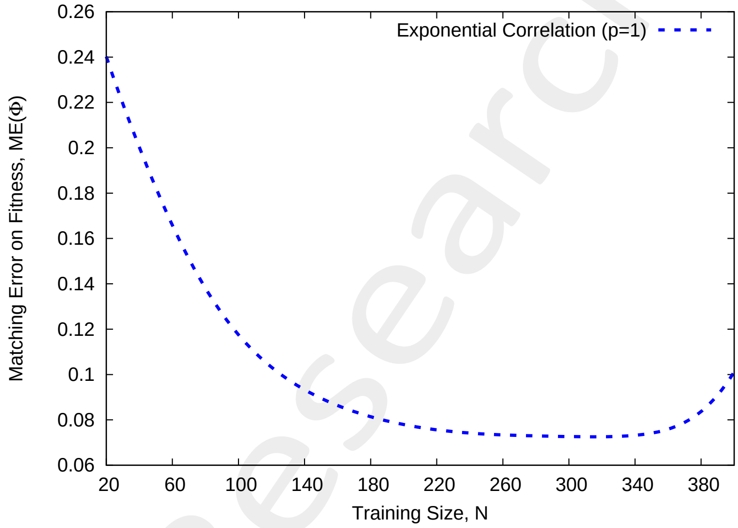

(b) ME

Figure 9: Plot of (a) Normalized Mean Error (NME) and (b) Matching Error (ME) vs training size (N) when considering an incremental training with random selection of N_l training samples form a set of S available simulations and testing the corresponding Kriging model on a test set made by the remaining $M_l = (S - N_l)$ simulations.

	Exponential Correlation	
N	NME	ME
20	6.49×10^{-1}	2.40×10^{-1}
80	4.32×10^{-1}	1.25×10^{-1}
140	2.92×10^{-1}	9.22×10^{-2}
200	2.84×10^{-1}	7.40×10^{-2}
300	2.41×10^{-1}	6.98×10^{-2}
400	2.37×10^{-1}	1.01×10^{-1}

Table XII: Normalized Mean Error (NME) and Matching Error (ME) vs training size (N).

2.0.5 Time Saving Analysis

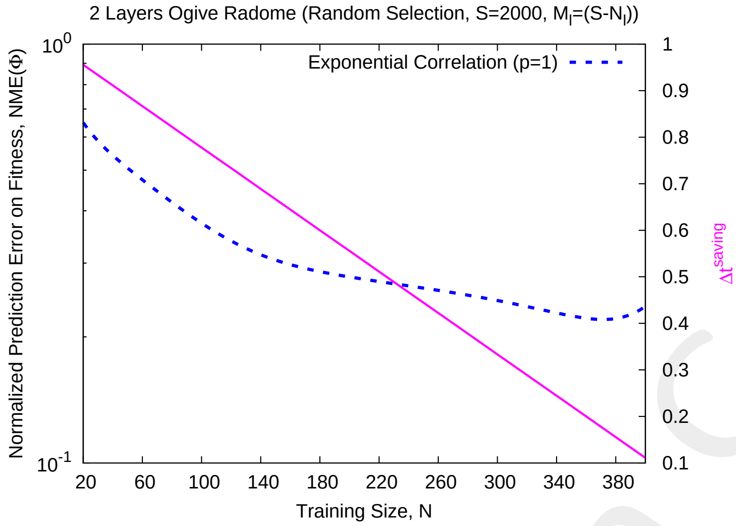

(a) NME

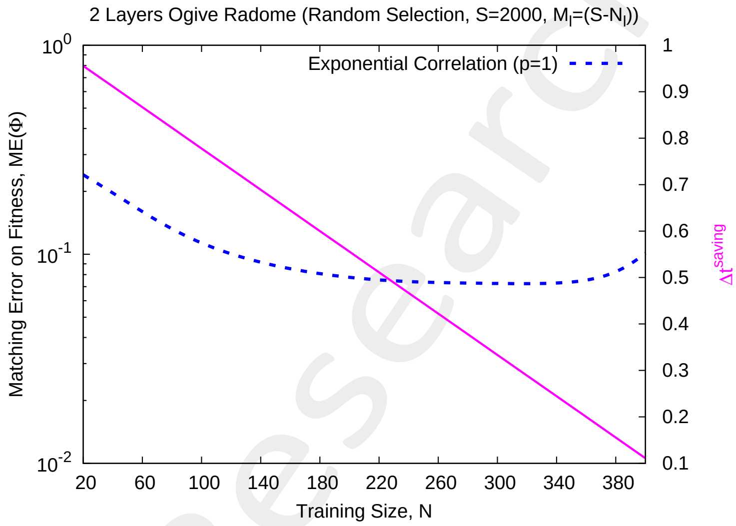

(b) ME

Figure 10: Plot of Time Saving (Δt^{saving}) with (a) Normalized Mean Error (NME) and (b) Matching Error (ME) vs training size (N) when considering an incremental training with random selection of N_l training samples form a set of S available simulations and testing the corresponding Kriging model on a test set made by the remaining $M_l = (S - N_l)$ simulations.

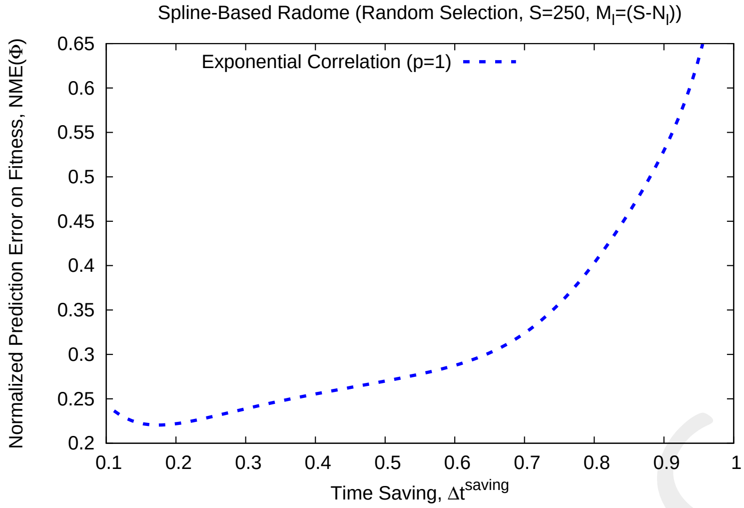

(a) NME

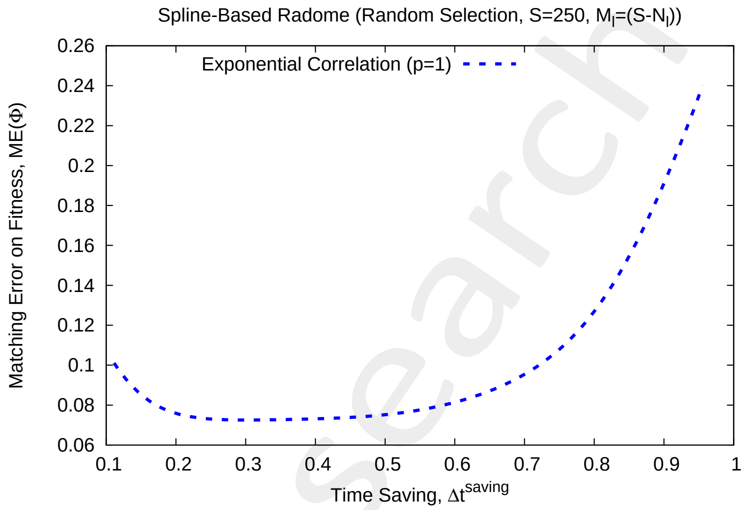

(b) ME

Figure 11: Plot of (a) Normalized Mean Error (NME) and (b) Matching Error (ME) vs Time Saving (Δt^{saving}).

2.0.6 Comparative assessment (Narrow Bounds vs Wide Bounds Training)

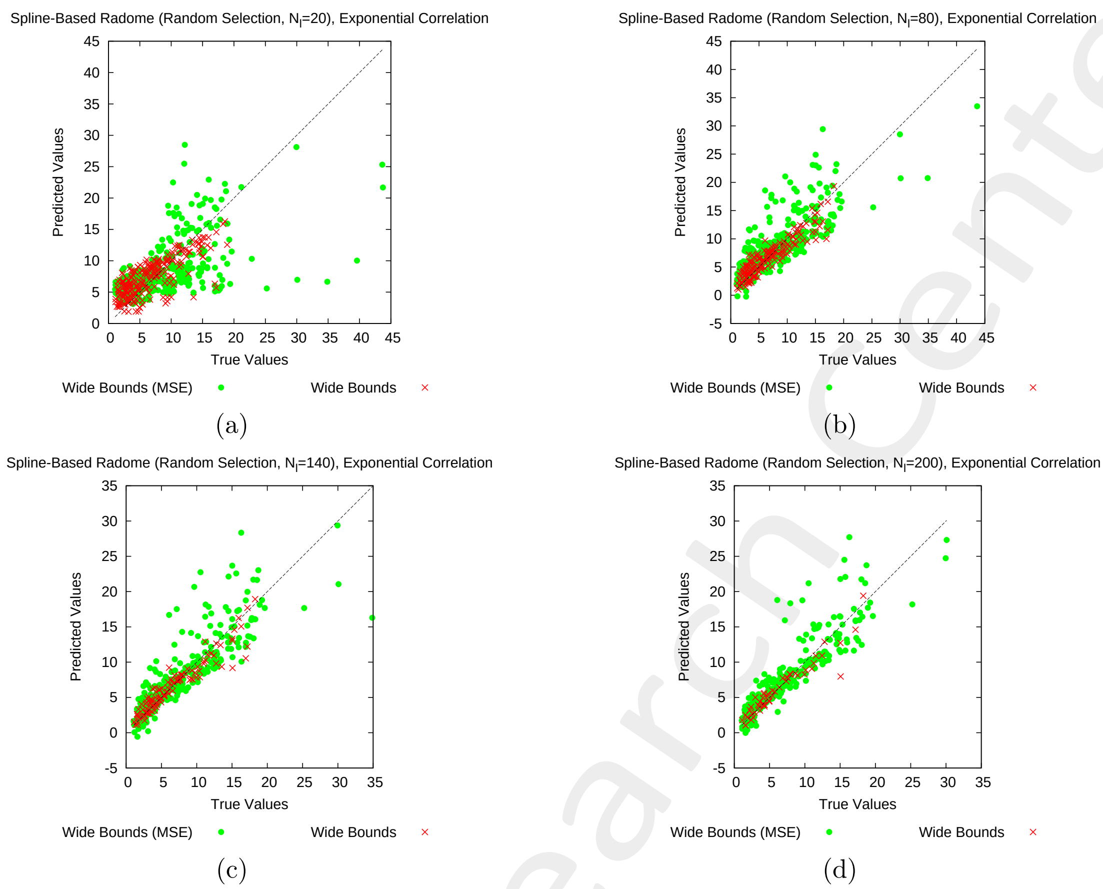

Figure 12: Plot of predicted vs actual values or different training sizes (N): (a) $N = 20$, (b) $N = 80$, (c) $N = 140$ and (d) $N = 200$.

Exponential Correlation

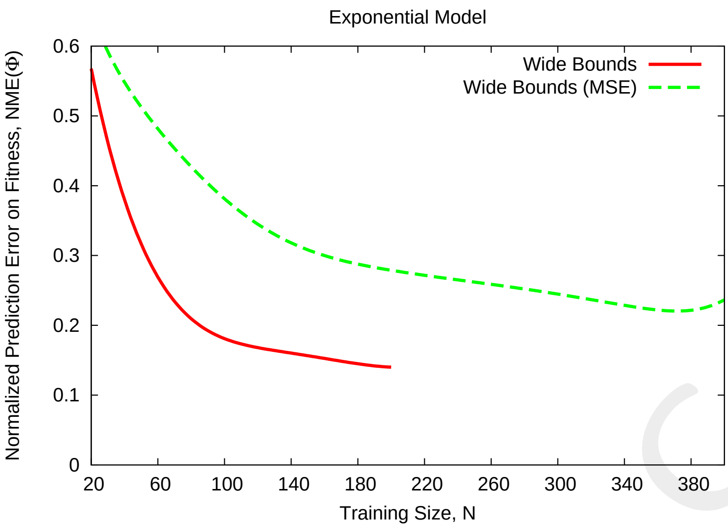

(b)

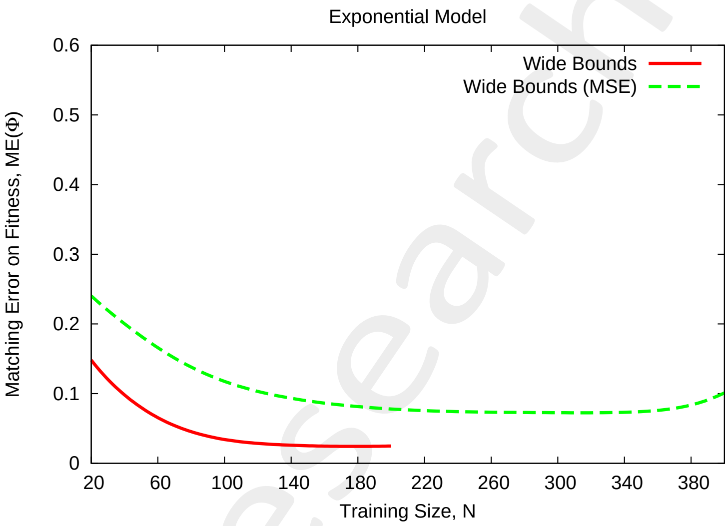

(d)

Figure 13: Plot of (a) Normalized Mean Error (NME) and (b) Matching Error (ME) vs training size (N) when considering an incremental training with random selection of N_l training samples form a set of S available simulations and testing the corresponding Kriging model on a test set made by the remaining $M_l = (S - N_l)$ simulations.

More information on the topics of this document can be found in the following list of references.

References

[1] A. Massa, D. Marcantonio, X. Chen, M. Li, and M. Salucci, “DNNs as applied to electromagnetics, antennas, and propagation - A review," *IEEE Antennas and Wirel. Propag. Lett.,* vol. 18, no. 11, pp. 2225-2229, Nov. 2019.

[2] A. Massa, G. Oliveri, M. Salucci, N. Anselmi, and P. Rocca, “Learning-by-examples techniques as applied to electromagnetics," *Journal of Electromagnetic Waves and Applications, Invited Review Article*, pp. 1-16, 2017.

[3] G. Oliveri, M. Salucci, and A. Massa, “Towards reflectarray digital twins - An EM-driven machine learning perspective,” *IEEE Trans. Antennas Propag. - Special Issue on 'Machine Learning in Antenna Design, Modeling, and Measurements*', vol. 70, no. 7, pp. 5078-5093, July 2022.

[4] M. Salucci, L. Tenuti, G. Oliveri, and A. Massa, “Efficient prediction of the EM response of reflectarray antenna elements by an advanced statistical learning method," *IEEE Trans. Antennas Propag.*, vol. 66, no. 8, pp. 3995-4007, Aug. 2018.

[5] M. Salucci, G. Oliveri, M. A. Hannan, and A. Massa, “System-by-design paradigm-based synthesis of complex systems: The case of spline-contoured 3D radomes,” *IEEE Antennas and Propagation Magazine - Special Issue on 'Artificial Intelligence in Electromagnetics,*', vol. 64, no. 1, pp. 72-83, Feb. 2022.

[6] G. Oliveri, P. Rocca, M. Salucci, and A. Massa, “Holographic smart EM skins for advanced beam power shaping in next generation wireless environments," *IEEE J. Multiscale Multiphysics Comput. Tech.*, vol. 6, pp. 171-182, Oct. 2021.

[7] G. Oliveri, A. Gelmini, A. Polo, N. Anselmi, and A. Massa, “System-by-design multi-scale synthesis of task-oriented reflectarrays," *IEEE Trans. Antennas Propag.*, vol. 68, no. 4, pp. 2867-2882, Apr. 2020.

[8] M. Salucci, L. Tenuti, G. Gottardi, A. Hannan, and A. Massa, “System-by-design method for efficient linear array miniaturisation through low-complexity isotropic lenses" *Electronic Letters*, vol. 55, no. 8, pp. 433-434, May 2019.

[9] M. Salucci, N. Anselmi, S. Goudos, and A. Massa, “Fast design of multiband fractal antennas through a system-by-design approach for NB-IoT applications," *EURASIP J. Wirel. Commun. Netw.*, vol. 2019, no. 1, pp. 68-83, Mar. 2019.

[10] M. Salucci, G. Oliveri, N. Anselmi, and A. Massa, “Material-by-design synthesis of conformal miniaturized linear phased arrays," *IEEE Access*, vol. 6, pp. 26367-26382, 2018.

[11] M. Salucci, G. Oliveri, N. Anselmi, G. Gottardi, and A. Massa, "Performance enhancement of linear active electronically-scanned arrays by means of MbD-synthesized metalenses," *Journal of Electromagnetic Waves and Applications*, vol. 32, no. 8, pp. 927-955, 2018.

[12] G. Oliveri, M. Salucci, N. Anselmi and A. Massa, "Multiscale System-by-Design synthesis of printed WAIMs for waveguide array enhancement," *IEEE J. Multiscale Multiphysics Computat. Techn.*, vol. 2, pp. 84-96, 2017.

[13] A. Massa and G. Oliveri, "Metamaterial-by-Design: Theory, methods, and applications to communications and sensing - Editorial," *EPJ Applied Metamaterials*, vol. 3, no. E1, pp. 1-3, 2016.

[14] G. Oliveri, F. Viani, N. Anselmi, and A. Massa, "Synthesis of multi-layer WAIM coatings for planar phased arrays within the system-by-design framework," *IEEE Trans. Antennas Propag.*, vol. 63, no. 6, pp. 2482-2496, June 2015.

[15] G. Oliveri, L. Tenuti, E. Bekele, M. Carlin, and A. Massa, "An SbD-QCTO approach to the synthesis of isotropic metamaterial lenses" *IEEE Antennas Wireless Propag. Lett.*, vol. 13, pp. 1783-1786, 2014.

[16] A. Massa, G. Oliveri, P. Rocca, and F. Viani, "System-by-Design: a new paradigm for handling design complexity," *8th European Conference on Antennas Propag. (EuCAP 2014), The Hague, The Netherlands*, pp. 1180-1183, Apr. 6-11, 2014.

[17] P. Rocca, M. Benedetti, M. Donelli, D. Franceschini, and A. Massa, "Evolutionary optimization as applied to inverse problems," *Inverse Problems - 25 th Year Special Issue of Inverse Problems, Invited Topical Review*, vol. 25, pp. 1-41, Dec. 2009.

[18] P. Rocca, G. Oliveri, and A. Massa, "Differential Evolution as applied to electromagnetics," *IEEE Antennas Propag. Mag.*, vol. 53, no. 1, pp. 38-49, Feb. 2011.

[19] P. Rocca, N. Anselmi, A. Polo, and A. Massa, "Pareto-optimal domino-tiling of orthogonal polygon phased arrays," *IEEE Trans. Antennas Propag.*, vol. 70, no. 5, pp. 3329-3342, May 2022.

[20] P. Rocca, N. Anselmi, A. Polo, and A. Massa, "An irregular two-sizes square tiling method for the design of isophoric phased arrays," *IEEE Trans. Antennas Propag.*, vol. 68, no. 6, pp. 4437-4449, Jun. 2020.

[21] P. Rocca, N. Anselmi, A. Polo, and A. Massa, "Modular design of hexagonal phased arrays through diamond tiles," *IEEE Trans. Antennas Propag.*, vol.68, no. 5, pp. 3598-3612, May 2020.

[22] N. Anselmi, L. Poli, P. Rocca, and A. Massa, "Design of simplified array layouts for preliminary experimental testing and validation of large AESAs," *IEEE Trans. Antennas Propag.*, vol. 66, no. 12, pp. 6906-6920, Dec. 2018.

[23] N. Anselmi, P. Rocca, M. Salucci, and A. Massa, "Contiguous phase-clustering in multibeam-on-receive scanning arrays," *IEEE Trans. Antennas Propag.*, vol. 66, no. 11, pp. 5879-5891, Nov. 2018.

[24] G. Oliveri, G. Gottardi, F. Robol, A. Polo, L. Poli, M. Salucci, M. Chuan, C. Massagrande, P. Vinetti, M. Mattivi, R. Lombardi, and A. Massa, “Co-design of unconventional array architectures and antenna elements for 5G base station," *IEEE Trans. Antennas Propag.*, vol. 65, no. 12, pp. 6752-6767, Dec. 2017.

[25] N. Anselmi, P. Rocca, M. Salucci, and A. Massa, “Irregular phased array tiling by means of analytic schemata-driven optimization," *IEEE Trans. Antennas Propag.*, vol. 65, no. 9, pp. 4495-4510, Sept. 2017.

[26] N. Anselmi, P. Rocca, M. Salucci, and A. Massa, “Optimization of excitation tolerances for robust beamforming in linear arrays" *IET Microwaves, Antennas & Propagation*, vol. 10, no. 2, pp. 208-214, 2016.

[27] P. Rocca, R. J. Mailloux, and G. Toso, “GA-Based optimization of irregular sub-array layouts for wideband phased arrays desig," *IEEE Antennas and Wireless Propag. Lett.*, vol. 14, pp. 131-134, 2015.

[28] P. Rocca, M. Donelli, G. Oliveri, F. Viani, and A. Massa, “Reconfigurable sum-difference pattern by means of parasitic elements for forward-looking monopulse radar," *IET Radar, Sonar & Navigation*, vol 7, no. 7, pp. 747-754, 2013.

[29] P. Rocca, L. Manica, and A. Massa, “Ant colony based hybrid approach for optimal compromise sum-difference patterns synthesis," *Microwave Opt. Technol. Lett.*, vol. 52, no. 1, pp. 128-132, Jan. 2010.

[30] P. Rocca, L. Manica, and A. Massa, “An improved excitation matching method based on an ant colony optimization for suboptimal-free clustering in sum-difference compromise synthesis," *IEEE Trans. Antennas Propag.*, vol. 57, no. 8, pp. 2297-2306, Aug. 2009.

[31] N. Anselmi, L. Poli, P. Rocca, and A. Massa, “Design of simplified array layouts for preliminary experimental testing and validation of large AESAs," *IEEE Trans. Antennas Propag.*, vol. 66, no. 12, pp. 6906-6920, Dec. 2018.

[32] M. Salucci, F. Robol, N. Anselmi, M. A. Hannan, P. Rocca, G. Oliveri, M. Donelli, and A. Massa, “S-Band spline-shaped aperture-stacked patch antenna for air traffic control applications," *IEEE Trans. Antennas Propag.*, vol. 66, no. 8, pp. 4292-4297, Aug. 2018.

[33] F. Viani, F. Robol, M. Salucci, and R. Azaro, “Automatic EMI filter design through particle swarm optimization," *IEEE Trans. Electromagnet. Compat.*, vol. 59, no. 4, pp. 1079-1094, Aug. 2017.